

ОБЪЕДИНЕННЫЙ  
ИНСТИТУТ  
ЯДЕРНЫХ  
ИССЛЕДОВАНИЙ

Дубна

E1-2008-7

A. Artikov<sup>1,2</sup>, G. Bellettini<sup>3</sup>, J. Budagov<sup>1</sup>, G. Chlachidze<sup>1,4</sup>,  
D. Chokheli<sup>1,5</sup>, V. Glagolev<sup>1</sup>, O. Pukhov<sup>1</sup>, A. Sissakian<sup>1</sup>,  
I. Suslov<sup>1</sup>, M. Trovato<sup>3</sup>, G. Velev<sup>4</sup>  
(on behalf of the CDF Collaboration)

TOP-QUARK MASS MEASUREMENT IN THE  $2.1 \text{ fb}^{-1}$   
TIGHT LEPTON AND ISOLATED TRACK SAMPLE  
USING NEUTRINO  $\phi$  WEIGHTING METHOD

---

<sup>1</sup> Joint Institute for Nuclear Research, Dubna, Russia

<sup>2</sup> On leave from NPL, Samarkand State University, Uzbekistan

<sup>3</sup> INFN and Department of Physics, University of Pisa, Italy

<sup>4</sup> FNAL, Batavia, USA

<sup>5</sup> On leave from HEPI, Tbilisi State University, Georgia

2008

Артиков А. и др. (по поручению коллаборации CDF) E1-2008-7  
Измерение массы топ-кварка на статистике  $2,1 \text{ fb}^{-1}$   
в событиях «лептон–трек» с помощью метода взвешивания  
по азимутальным углам нейтрино

С помощью метода взвешивания по азимутальным углам нейтрино измерена масса топ-кварка в событиях, содержащих хорошо выделенные лептон и заряженный трек. После применения соответствующих критериев отобрано 236 событий для интегральной светимости данных  $2,1 \text{ fb}^{-1}$ . Эти события реконструированы согласно  $t\bar{t}$ -гипотезе и отфитированы суперпозицией распределений сигнала и фона. Для ожидаемой величины фоновых событий  $105,8 \pm 12,9$  измерена масса топ-кварка  $M_{\text{top}} = 167,7 \pm_{4,0}^{4,2}$  (стат.)  $\pm 3,1$  (сист.)  $\text{ГэВ}/c^2$ .

Работа выполнена в Лаборатории ядерных проблем им. В. П. Дзепова ОИЯИ.

Сообщение Объединенного института ядерных исследований. Дубна, 2008

Artikov A. et al. (on behalf of the CDF Collaboration) E1-2008-7  
Top-Quark Mass Measurement in the  $2.1 \text{ fb}^{-1}$  Tight Lepton  
and Isolated Track Sample Using Neutrino  $\phi$  Weighting Method

We report on a measurement of the top quark mass in the tight lepton and isolated track sample using the neutrino  $\phi$  weighting method. After applying the selection cuts for the data sample with the integrated luminosity of  $2.1 \text{ fb}^{-1}$  236 events were obtained. These events were reconstructed according to the  $t\bar{t}$  hypothesis and fitted as a superposition of signal and combined background. For the expected number of background  $105.8 \pm 12.9$  we measure the top quark mass to be  $M_{\text{top}} = 167.7 \pm_{4.0}^{4.2}$  (stat.)  $\pm 3.1$  (syst.)  $\text{GeV}/c^2$ .

The investigation has been performed at the Dzhelapov Laboratory of Nuclear Problems, JINR.

Communication of the Joint Institute for Nuclear Research. Dubna, 2008

## 1. INTRODUCTION

In this paper, we present a top mass measurement in the *dilepton* channel using the neutrino  $\phi$  weighting algorithm (PHI). This method was successfully applied twice to the CDF II data: at the statistics of  $190 \text{ pb}^{-1}$  and later on at the statistics of  $340 \text{ pb}^{-1}$  [1].

Brief description of this method is given below. Some changes in  $\chi^2$ , compared to the previous analysis, were applied as further method development. In order to increase the statistical resolution we modified the  $\chi^2$  including the dependence of  $t$ -quark width vs.  $M_t$ . Also the transfer functions were applied for more accurate description of  $b$ -parton responses.

The integrated luminosity of the data sample is  $2.1 \text{ fb}^{-1}$ . Information about  $b$ -tag was not used in this analysis. Monte Carlo (MC) samples were produced by 6th generation of the CDF simulation and reconstruction programs.

For this analysis we applied the lepton + track event selection to collect more events due to the relaxed cuts for one of the leptons.

## 2. PRINCIPLES OF THE METHOD

**2.1. Constrained Variables.** We have unconstrained kinematic situation for the PHI method: a total number of 24 unknown ( $b, \bar{b}, l^-, l^+, \nu, \bar{\nu}$  4-momenta) and only 23 equations (measured 3-momenta for two  $b$ -jets and two leptons, assumed knowing mass for 6 final particles, used two transverse components of calorimeter missing energy, constrained invariant mass for two  $W$  and assumed equal constrained mass of top and antitop quarks) to constrain the kinematics.

Obviously, it is impossible to pick up directly only one solution per event. We must assume some of the event parameters ( $\mathbf{R}$ ) in order to constrain the kinematics and then vary the  $\mathbf{R}$  to determine the variety of solutions. In addition, every solution must have a weight attached to it.

The minimal requirement in the case of  $-1C$  kinematics to perform the  $\chi^2$  minimization is to use a two-dimensional vector as  $\mathbf{R}$ . For our analysis we choose the azimuthal angles of the neutrino momenta  $\mathbf{R} = (\phi_{\nu 1}, \phi_{\nu 2})$  and create a net of solutions in the  $(\phi_{\nu 1}, \phi_{\nu 2})$  plane.

**2.2. FITTER Procedure.** In this section we will clarify the idea about the tool called FITTER. The FITTER receives as input a set of information about a selected event and gives at output array of the reconstructed top quark masses with appropriate weights per event.

**2.2.1. The  $\chi^2$  form.** The FITTER uses final particles momentum, jet energy information as well as constraints on  $W$  and  $t$  masses. The common formula for  $\chi^2$  is

$$\chi^2 \equiv -2 \ln(\mathcal{P}(\mathbf{x})), \quad (1)$$

where  $\mathbf{x}$  is a general notation to indicate a variable and  $\mathcal{P}$  – its probability density distribution.

The expanded formula for  $\chi^2$  is

$$\begin{aligned}
\chi^2 &= \chi_{\text{res}}^2 + \chi_{\text{constr}}^2, \\
\chi_{\text{res}}^2 &= \sum_{l=1}^2 \frac{(P_T^l - \widetilde{P}_T^l)^2}{\sigma_{P_T}^l{}^2} + \sum_{j=1}^2 [-2 \ln(\mathcal{P}_{tf}(\widetilde{P}_T^j | P_T^j))] + \\
&\quad + \sum_{i=x,y} \frac{(UE^i - \widetilde{UE}^i)^2}{\sigma_{UE}^i{}^2}, \\
\chi_{\text{constr}}^2 &= -2 \ln(\mathcal{P}_{BW}(m_{\text{inv}}^{l_1, \nu_1} | M_W, \Gamma_{M_W})) - \\
&\quad - 2 \ln(\mathcal{P}_{BW}(m_{\text{inv}}^{l_2, \nu_2} | M_W, \Gamma_{M_W})) - \\
&\quad - 2 \ln(\mathcal{P}_{BW}(m_{\text{inv}}^{l_1, \nu_1, j_1} | \widetilde{M}_t, \Gamma_{\widetilde{M}_t})) - \\
&\quad - 2 \ln(\mathcal{P}_{BW}(m_{\text{inv}}^{l_2, \nu_2, j_2} | \widetilde{M}_t, \Gamma_{\widetilde{M}_t})).
\end{aligned} \tag{2}$$

The variables with a tilde sign refer to the output of the minimization procedure, whereas  $P_T$  and  $UE$  (unclustered energy) represent measured values corrected for known detector and physics effects.  $M_t$  is the fit parameter giving the reconstructed top mass.  $BW$  and  $tf$  are the relativistic Breit–Wigner and transfer functions, respectively.

Notice that we splitted the  $\chi^2$  into two parts: the first one,  $\chi_{\text{res}}^2$ , takes into account the detector uncertainties, whereas the second one deals with the known mass constraints.

The first sum (in  $\chi_{\text{res}}^2$ ) runs over the primary lepton (tight lepton) and the track lepton. We take the uncertainties for the lepton and track lepton from the Run I studies [2]:

$$\frac{\sigma_{P_T}^e}{P_T^e} = \sqrt{\frac{a}{P_T^e} + b}, \tag{3}$$

$$\frac{\sigma_{P_T}^\mu}{P_T^\mu} = c P_T^\mu, \tag{4}$$

where  $a = 0.135^2$ ,  $b = 0.02^2$ ,  $c = 0.0011$ .

The second sum (in  $\chi_{\text{res}}^2$ ) is over the two leading jets.

The third sum (in  $\chi_{\text{res}}^2$ ) is over the two transverse components of the unclustered energy<sup>1</sup>.

The other term in formula (2),  $\chi_{\text{constr}}^2$ , refers to the invariant masses of the couples lepton–neutrino and the lepton–neutrino–leading jet system. We set

---

<sup>1</sup> $UE$  is defined as the sum of all unclustered energy in the calorimeter, that is the sum of all towers which are not associated with any of the objects previously considered in the  $\chi^2$  formula (tight lepton, track lepton, two leading jets): notice that this definition also includes remaining jets with  $E_T > 8$  GeV and  $|\eta| < 2$  which are not already taken into account as leading jets.

$M_W = 80.41 \text{ GeV}/c^2$ ,  $\Gamma_{M_W} = 2.06 \text{ GeV}/c^2$  and insert the function  $\Gamma_{M_t}$  (see Fig. 1), according to the Standard Model [3].

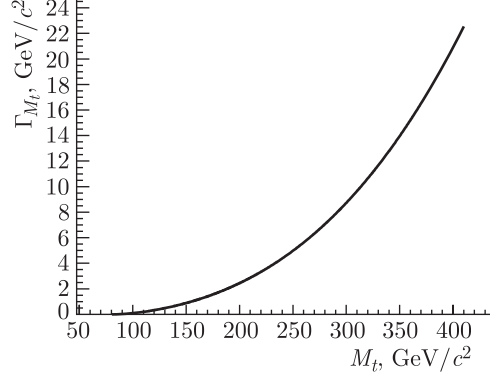


Fig. 1. Top width vs. top mass

The insertion of the top width dependence from the top mass is new for our analysis. We will discuss obtained improvement later in this paper.

**2.2.2. Scanning of the  $(\phi_1, \phi_2)$  plane.** We should find the solutions over the  $(\phi_1, \phi_2)$  variety: we optimized the step [1] and we scan all the  $(0, 2\pi) \times (0, 2\pi)$   $(\phi_1, \phi_2)$  net. The net is chosen to have  $12 \times 12$  points for  $(0, \pi) \times (0, \pi)$   $(\phi_1, \phi_2)$ . For each point of the net we can write the following linear system:

$$\begin{cases} P_T^{\nu 1} \cos(\phi_{\nu 1}) + P_T^{\nu 2} \cos(\phi_{\nu 2}) = \cancel{E}_{T_x}, \\ P_T^{\nu 1} \sin(\phi_{\nu 1}) + P_T^{\nu 2} \sin(\phi_{\nu 2}) = \cancel{E}_{T_y}, \end{cases} \quad (5)$$

which is solved by

$$\begin{cases} P_x^{\nu 1} \equiv P_T^{\nu 1} \cos(\phi_{\nu 1}) = \frac{\cancel{E}_{T_x} \sin(\phi_{\nu 2}) - \cancel{E}_{T_y} \cos(\phi_{\nu 2})}{\sin(\phi_{\nu 2} - \phi_{\nu 1})} \cos(\phi_{\nu 1}), \\ P_y^{\nu 1} \equiv P_T^{\nu 1} \sin(\phi_{\nu 1}) = \frac{\cancel{E}_{T_x} \sin(\phi_{\nu 2}) - \cancel{E}_{T_y} \cos(\phi_{\nu 2})}{\sin(\phi_{\nu 2} - \phi_{\nu 1})} \sin(\phi_{\nu 1}), \\ P_x^{\nu 2} \equiv P_T^{\nu 2} \cos(\phi_{\nu 2}) = \frac{\cancel{E}_{T_x} \sin(\phi_{\nu 1}) - \cancel{E}_{T_y} \cos(\phi_{\nu 1})}{\sin(\phi_{\nu 1} - \phi_{\nu 2})} \cos(\phi_{\nu 2}), \\ P_y^{\nu 2} \equiv P_T^{\nu 2} \sin(\phi_{\nu 2}) = \frac{\cancel{E}_{T_x} \sin(\phi_{\nu 1}) - \cancel{E}_{T_y} \cos(\phi_{\nu 1})}{\sin(\phi_{\nu 1} - \phi_{\nu 2})} \sin(\phi_{\nu 2}). \end{cases} \quad (6)$$

Since we add two additional values, we perform a 1C fit minimization of the  $\chi^2$  (2). This is done for every point of the net, with a particular attention to avoid those ones satisfying the equation  $\phi_{\nu 1} - \phi_{\nu 2} = k\pi$  with  $k = 0, 1$  (in practice there is no limitation because we optimize the net by avoiding these points).

We must notice that we would have the same components of the neutrino's momentum  $P_{x,y}^{\nu 1, \nu 2}$  for  $\phi'_{\nu 1, \nu 2} = \phi_{\nu 1, \nu 2} + \pi$  (see (6)) and we would take into account three unphysical solutions ( $P_T^{\nu 1} < 0$  and/or  $P_T^{\nu 2} < 0$ ). To subdivide the whole net we should scan  $(0, 2\pi) \times (0, 2\pi)$  into 4 areas:  $(0, \pi) \times (0, \pi)$ ,  $(0, \pi) \times (\pi, 2\pi)$ ,  $(\pi, 2\pi) \times (0, \pi)$ ,  $(\pi, 2\pi) \times (\pi, 2\pi)$ .

We stay away from the unphysical solutions by scanning a  $(0, \pi)(0, \pi)$  net and by changing sign to  $P_T^{\nu 1(\nu 2)}$  in the case to find the negative neutrino momentum. This automatically changes the  $\phi$  quadrant as shown by the equation:

$$\phi'_{\nu 1(\nu 2)} = \phi_{\nu 1(\nu 2)} + \pi \implies P'_{x,y}{}^{\nu 1(\nu 2)} = P_{x,y}{}^{\nu 1(\nu 2)} \text{ and } P'_T{}^{\nu 1(\nu 2)} = -P_T{}^{\nu 1(\nu 2)}.$$

Starting from the 8 solutions per net point per event (longitudinal momentum component for every neutrino has two solutions and there is an ambiguity in coupling  $W$  with  $b$ -jets) we can finally say that we have to do 1152 1C minimizations which return the  $\widehat{M}_{t_{ijk}}$  and  $\chi^2_{ijk}$  ( $i = 1, \dots, 12; j = 1, \dots, 12; k = 1, \dots, 8$ ) at the output.

**2.2.3. Weighting the solutions.** In Subsec. 2.2.1 we apply the Breit–Wigner functions inside the  $\chi^2$  (formula (2)) for  $W$  and  $t$  invariant mass distributions. The relativistic Breit–Wigner formula is

$$BW(m_{\text{inv}} | m, \Gamma) \sim \frac{1}{(m_{\text{inv}}^2 - m^2)^2 + m^2 \Gamma^2}. \quad (7)$$

For our analysis we decided to use the next Breit–Wigner normalization to obtain the top mass solutions:

$$BW(m_{\text{inv}} | m, \Gamma) = \frac{\Gamma^2 \cdot m^2}{(m_{\text{inv}}^2 - m^2)^2 + m^2 \Gamma^2}, \quad (8)$$

where  $m$  and  $\Gamma$  are the mass and the decay width for  $t$  or  $W$  particles, depending on the considered decay chain;  $m_{\text{inv}}$  refers to the invariant mass, calculated with the appropriate information from lepton and neutrino, in case of  $W$  decay, or lepton, neutrino and leading jet, in case of  $t$  decay.

In case of  $W \rightarrow l\nu$  Breit–Wigner, formula (8) has a constant decay width, which has not any importance in the  $\chi^2$  minimization. Instead of  $\Gamma_t$  depends on the  $\chi^2$  minimization parameter (top mass, see Fig. 1).

Our investigation shows that the distribution of reconstructed masses has the smaller error and the more accurate mean value if we apply for the solutions weights the renormalized Breit–Wigner formula:

$$BW(m_{\text{inv}} | m, \Gamma) = \frac{\Gamma \cdot m^2}{(m_{\text{inv}}^2 - m^2)^2 + m^2 \Gamma^2}. \quad (9)$$

This function is normalized to 1, instead of the previous one, which has the maximum independent of the top mass (see Fig. 2). We select the lowest  $\chi^2$  solution out of (8) with associated mass for every point of the  $(\phi_1, \phi_2)$  net, this way we reduce the number of obtained masses to 144 per event. Each of these masses should be taken into account because each of them arises from a particular and physical configuration of our event.

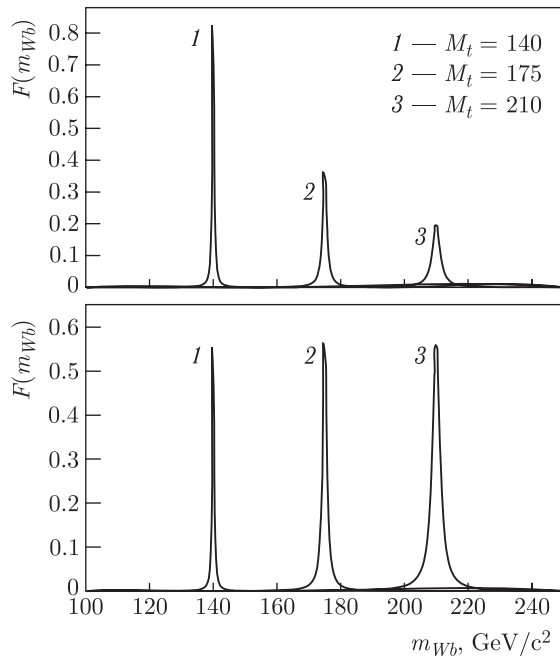


Fig. 2. The relativistic Breit-Wigner functions: top – equation (9), bottom – equation (8)

Then we are using the  $\chi^2$  definition (according to (9)) to give a probability of occurrence for our 144 solutions. The expression for the weight is given below:

$$w_{ij} = \frac{e^{-\frac{\chi_{ij}^2}{2}}}{\sum_{i,j=1}^{12} e^{-\frac{\chi_{ij}^2}{2}}}; \quad i, j = 1, \dots, 12. \quad (10)$$

This formula is obtained by inverting (1) and normalized by 1.

**2.3. Picking up the Solution.** Once we have found the weight for each of the 144 masses per event, we define an optimized procedure to obtain the final reconstructed mass per event. The procedure follows the steps below:

1. We build a mass probability density distribution (PDD) by using  $w_{ij}$  and  $\widetilde{M}_{t_{ij}}$  info: we have 144 entries per event.
2. We identify the most probable value (MPV).
3. We calculate  $M_t^{\text{rec}}$  by averaging the PDD bins with values above threshold of 0.3 from MPV which was optimized and described in [1].

**2.4. Likelihood Form.** The likelihood function finds the probability that our data candidates are described by an appropriate admixture of background events and dilepton  $t\bar{t}$  decays with a certain top quark mass.

We perform comparison by parametrizing the mass distributions in Monte Carlo templates, reconstructing the  $M_t^{\text{rec}}$  on the data sample and finally matching the two by using the likelihood unbinned fit and minimization.

The likelihood function has the following form:

$$\mathcal{L} = \mathcal{L}_{\text{shape}} \mathcal{L}_{\text{backgr}} \mathcal{L}_{\text{param}}, \quad (11)$$

where

$$\mathcal{L}_{\text{shape}} = \frac{e^{-(n_s+n_b)}(n_s+n_b)^N}{N!} \prod_{n=1}^N \frac{n_s f_s(m_n | M_{\text{top}}) + n_b f_b(m_n)}{n_s + n_b} \quad (12)$$

and

$$\mathcal{L}_{\text{backgr}} = \exp\left(-\frac{(n_b - n_b^{\text{exp}})^2}{2\sigma_{n_b}^2}\right), \quad (13)$$

$$\mathcal{L}_{\text{param}} = \exp\{-0.5[(\boldsymbol{\alpha} - \boldsymbol{\alpha}_0)^T U^{-1}(\boldsymbol{\alpha} - \boldsymbol{\alpha}_0) + (\boldsymbol{\beta} - \boldsymbol{\beta}_0)^T V^{-1}(\boldsymbol{\beta} - \boldsymbol{\beta}_0)]\}. \quad (14)$$

Here  $U$  and  $V$  are the covariance matrices for the parameters  $\boldsymbol{\alpha}_0$  and  $\boldsymbol{\beta}_0$ , respectively (see (15)–(18)).

The likelihood maximization procedure (we usually minimize  $-\ln(\mathcal{L})$ ) returns a *true top quark mass estimator*  $M_{\text{top}}$  and estimated numbers of signal ( $n_s$ ) and background ( $n_b$ ).

We assign a probability ( $f_s$ ) that each of the selected events looks like signal and a probability ( $f_b$ ) that this event can be considered as background one. These two probabilities are weighted according to appropriate signal and background numbers  $n_s$  and  $n_b$ .

Moreover, we want to point out that PHI method uncertainties in the signal and background parametrization are included directly into the statistical error estimation procedure.

### 3. PHI METHOD OPTIMIZATION

In this section we explain what are the improvements which were obtained by upgrading the  $\chi^2$  in formula (2) and the appropriate weights (see (10)).

Basically we introduced two changes in the definition of the  $\chi^2$ : 1) we switched from the approximate Gaussian functions for the invariant mass constraint [1] to the more physical correct Breit–Wigner distributions, concerning to  $t$ ,  $\bar{t}$ ,  $W^\pm$  decays, and 2) we use the  $m_t$  dependent  $\Gamma_t$  instead of the constant value used before [1].

We have compared the top mass spectra reconstructed by means of the slightly different functions for the Breit–Wigner (9) and (8) included in  $\chi^2$ .

In Fig. 3 the plots were built by using Monte Carlo information at parton level. Only one solution per event was picked up because we do not have any ambiguities about  $P_z^\nu$ ,  $(\phi_1, \phi_2)$  and lepton-jets pairings. Because of this reason, this check is weight-independent. Monte Carlo generated events with  $M_t = 161, 171$  and  $181 \text{ GeV}/c^2$  were used. The comparison shows the advantage of function (8) applied for  $\chi^2$  minimization. As a next step of optimization, we tried a different kind of weight applied to the top mass solutions.

We compared the different ways of reconstructing top invariant masses (see Fig. 4):

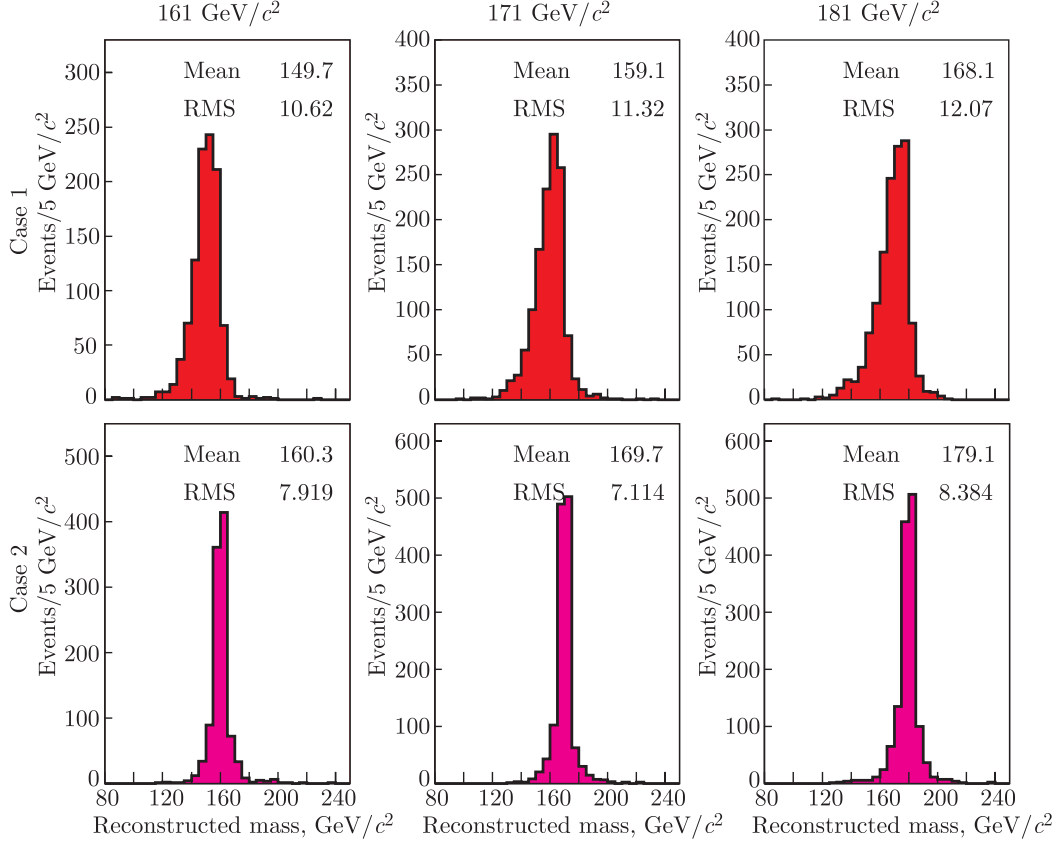


Fig. 3. Top mass reconstruction at HEPG level by using Breit-Wigner: (9) – top plots and (8) – bottom plots

- Case 0: Gaussian distribution function for both  $\chi^2$  and weight [1].
- Case A: Breit-Wigner's as in (8) for the  $\chi^2$  and for the weight.
- Case B: Breit-Wigner's as in (9) for the  $\chi^2$  and for the weight.
- Case C: Mixed combination: Breit-Wigner's as in (8) for the  $\chi^2$  and the weight recalculated according to Breit-Wigner function (9).

In Fig.4 we plotted the estimated statistical errors<sup>1</sup> calculated by using Monte Carlo generated  $t\bar{t}$  events with expected number of signal events  $n_s = 60.53$  versus input top quark mass.

The conclusion is clear: *The method C* is chosen as our final way since it has the best resolution. The resolution gain is about 20% as to compare to our previous method (Case 0).

<sup>1</sup> This error is obtained by performing the pseudo-experiments technique.

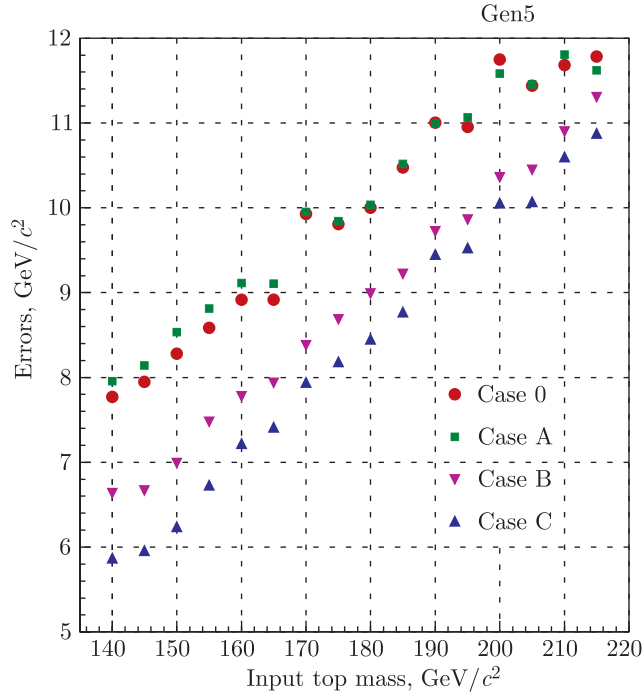


Fig. 4. Improvements in final statistical errors by using  $M_t$ -dependent Breit–Wigner functions and two different weights for the top mass solutions

Moreover, we changed the leading jet term inside equation (2). We switched from the formula  $\sum_{j=1}^2 \frac{(P_T^j - \tilde{P}_T^j)^2}{\sigma_{P_T}^j}$  ( $j$  runs over the two leading jets) to one that exploits our transfer function<sup>1</sup>.

Figure 5 represents the variable  $k = (P_T^{\text{part}} - P_T^{\text{jet}})/P_T^{\text{jet}}$ , fitted in different  $(|\eta|, P_T^{\text{jet}})$  regions.

For production of these plots we used Monte Carlo  $t\bar{t}$  events with top mass  $175, 175 \pm 0.5 \text{ GeV}/c^2$ . We take into account  $b$  parton  $P_T$  dependence from  $M_t$  by adding an appropriate weight.

We do not see a big gain in respect to the previous analysis [1], as shown in Fig. 6: blue dots refer to the procedure of top mass calculation performed by using transfer functions, and red ones are for the old type  $\chi^2$ , i.e., without these transfer functions.

#### 4. EVENT SELECTION

In our analysis we used data collected between March 2002 and May 2007, corresponding to a total integrated luminosity of  $2.1 \text{ fb}^{-1}$ . The data are collected with an inclusive lepton trigger that requires an electron with  $E_T > 18 \text{ GeV}$  or a

<sup>1</sup> Also called as «top specific corrections».

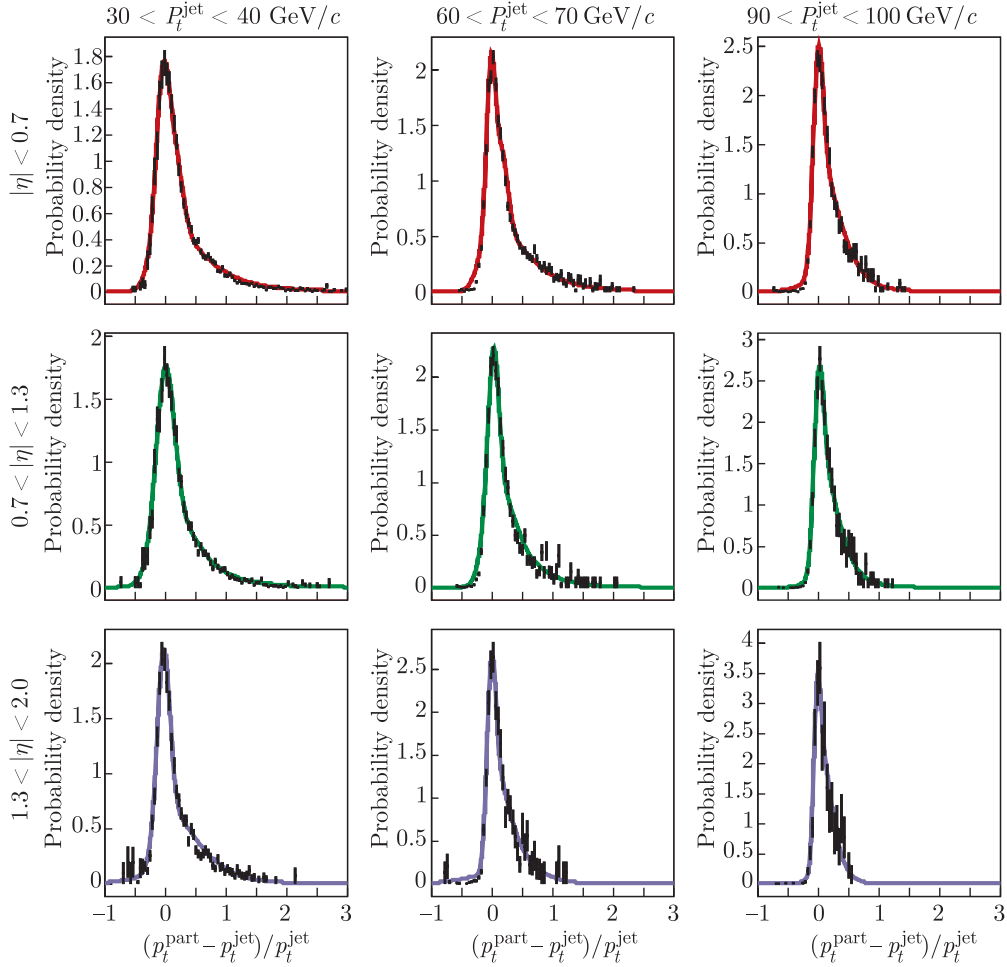


Fig. 5. Top specific corrections

muon with  $P_T > 18$  GeV/ $c$ . After full event reconstruction we select events with a tight electron  $E_T > 20$  GeV or muon with  $P_T > 20$  GeV/ $c$ , an isolated high- $p_t$  track  $P_T > 20$  GeV/ $c$  (track lepton or tl), two or more jets  $E_T > 20$  GeV, and significant  $\cancel{E}_T > 25$  GeV.

Tight electron candidates have a well-measured track pointing at an energy deposition in the calorimeter. In addition, the candidate's electromagnetic shower profile must be consistent with that expected for electrons. Tight muon candidates must have a well-measured track linked to hits in the muon chambers and energy deposition in the calorimeters consistent with that expected for muons. Tight lepton have to be isolated that means that the total transverse energy within cone  $\Delta R \equiv \sqrt{(\Delta \eta)^2 + (\Delta \phi)^2} < 0.4$ , minus the candidate lepton  $E_T$ , is less than 10% of the candidate lepton  $E_T$ .

To count as the second lepton (track lepton) for our analysis a well-measured track must have  $P_T > 20$  GeV/ $c$ , and pass a track isolation requirement. The

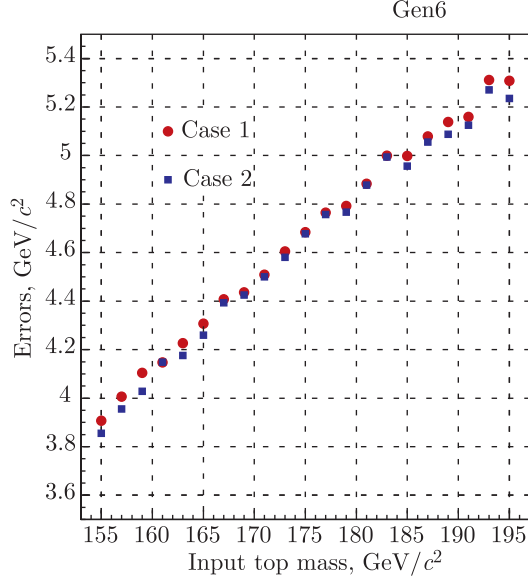


Fig. 6. Statistical error improvement by using top specific corrections

track isolation is defined as the ratio of the transverse momentum of the candidate track to the sum of the transverse momenta of all tracks in a cone of  $\Delta R \equiv \sqrt{(\Delta \eta)^2 + (\Delta \phi)^2} < 0.4$  around it, including the candidate track itself. The track isolation value should be  $> 0.9$ .

The tight lepton and the track lepton have to be oppositely charged.

Two (or more) jets with corrected  $E_T > 20$  GeV and  $|\eta| < 2.0$  are also required.

If  $\cancel{E} < 50$  GeV, we additionally require that the angle between  $\cancel{E}$  and the nearest jet is  $\Delta \phi > 25^\circ$ .

Events with cosmic ray, conversion or  $Z$  are eliminated.

After these selection cuts 236 events were left, which were reconstructed according to the  $t\bar{t}$  hypothesis. The same cuts were applied to the Monte Carlo generated signal or background events.

## 5. TEMPLATES

**5.1. Monte Carlo Signal Templates.** The official MC samples were used. The signal templates for input top masses in the  $155 \div 195$  GeV range were created with 2 GeV steps (see the examples in Fig. 7).

Then the obtained set of templates was parametrized by one Landau and two Gaussian functions

$$f_s(M_t^{\text{rec}} | M_{\text{top}}) = p_7(p_6 \frac{1}{\sqrt{2\pi} p_2} e^{-0.5(\frac{M_t^{\text{rec}} - p_1}{p_2} + e^{-\frac{M_t^{\text{rec}} - p_1}{p_2}})}) +$$

$$+ (1 - p_6) \frac{1}{\sqrt{2\pi} p_5} e^{-0.5 \left( \frac{M_t^{\text{rec}} - p_4}{p_5} \right)^2} + (1 - p_7) \frac{1}{\sqrt{2\pi} p_3} e^{-0.5 \left( \frac{M_t^{\text{rec}} - p_8}{p_3} \right)^2}. \quad (15)$$

Notice that this parametrizing function is strongly-dependent from the input top mass  $M_{\text{top}}$ , or, it is better to say, that its parameters  $p_1, \dots, p_8$ , are  $M_{\text{top}}$ -dependent:

$$p_k = \alpha_k + \alpha_{k+8} M_{\text{top}}. \quad (16)$$

**5.2. Background Template.** We used for background processes official Gen.6 MC samples ( $WZ \rightarrow ll$ ,  $WW \rightarrow ll$ ,  $ZZ \rightarrow ll$ , Drell-Yan,  $Z \rightarrow \tau\tau$ ).

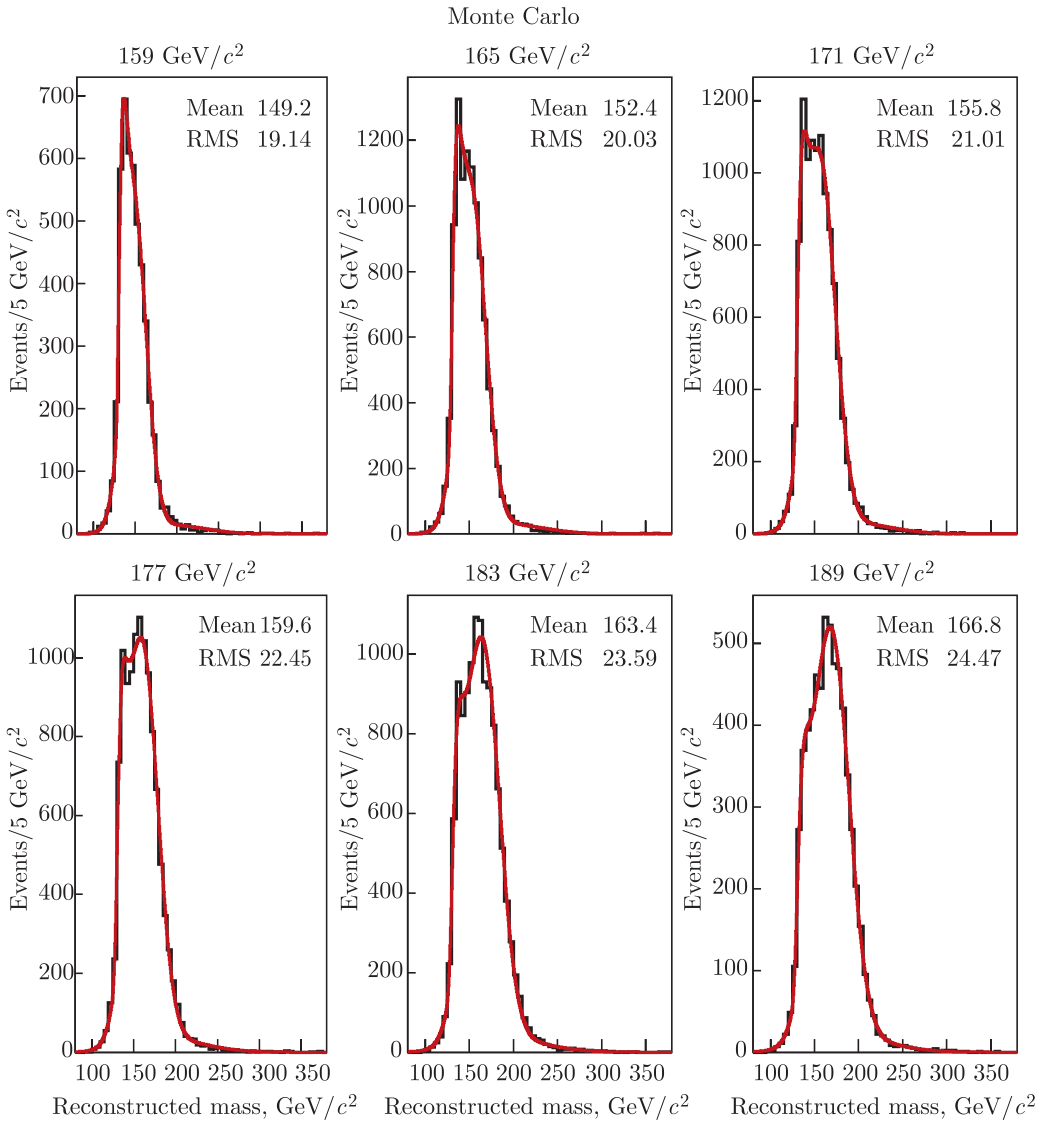


Fig. 7. The examples of the signal templates

Template for fake events was obtained by weighting the fakeable events from  $W$ +jets data sample according to the fake rate probability matrix. In order to build general template for Drell–Yan events the templates for each subprocess were combined using their cross sections and acceptances.

The obtained templates for these processes were combined together according to the expected number of events, as derived by the  $t\bar{t}$  cross-section group, we show these numbers in Table 1.

**Table 1. Predicted and observed events in  $1.1 \text{ fb}^{-1}$ , with details of the background contributions. The opposite charge requirement is applied**

	$n_j = 0$	$n_j = 1$	$n_j \geq 2$
$WW$	$91.66 \pm 7.54$	$15.96 \pm 1.34$	$3.90 \pm 0.36$
$WZ$	$10.00 \pm 0.83$	$4.55 \pm 0.38$	$1.43 \pm 0.13$
$ZZ$	$2.41 \pm 0.04$	$0.65 \pm 0.02$	$0.34 \pm 0.02$
$Z/\gamma^* \rightarrow ee$	$72.43 \pm 15.79$	$25.93 \pm 6.05$	$7.75 \pm 2.24$
$Z/\gamma^* \rightarrow \mu\mu$	$18.88 \pm 5.32$	$8.88 \pm 2.74$	$3.40 \pm 1.15$
$Z/\gamma^* \rightarrow \tau\tau$	$35.54 \pm 3.24$	$26.46 \pm 2.47$	$7.31 \pm 0.89$
<b>Fakes</b>	$244.09 \pm 46.41$	$76.79 \pm 14.59$	$29.85 \pm 5.86$
<b>Background</b>	$475.01 \pm 51.58$	$176.52 \pm 16.98$	$53.99 \pm 6.60$
$t\bar{t}, \sigma = 6.7 \text{ pb}$	$1.18 \pm 0.06$	$17.29 \pm 0.56$	$60.53 \pm 1.88$
<b>Predicted</b>	<b><math>476.19 \pm 31.58</math></b>	<b><math>176.52 \pm 16.98</math></b>	<b><math>114.51 \pm 7.00</math></b>
<b>Observed</b>	<b>443</b>	<b>187</b>	<b>129</b>

The templates for different background components along with the combined background template are shown in Fig. 8.

The fitting function,  $f_b$ , is a slightly bit different from that used for signal templates, as one can see from the formula:

$$\begin{aligned}
f_b(M_t^{\text{rec}}) = & q_7(q_6 \frac{1}{\sqrt{2\pi} q_2} e^{-0.5(\frac{M_t^{\text{rec}}-q_1}{q_2} + e^{-\frac{M_t^{\text{rec}}-q_1}{q_2}})}) + \\
& + (1 - q_6) \frac{1}{\sqrt{2\pi} q_5} e^{-0.5(\frac{M_t^{\text{rec}}-q_4}{q_5})^2} + (1 - q_7) \frac{1}{\sqrt{2\pi} q_3} e^{-0.5(\frac{M_t^{\text{rec}}-q_8}{q_3} + e^{-\frac{M_t^{\text{rec}}-q_8}{q_3}})}.
\end{aligned} \tag{17}$$

However, the main difference from  $f_s$  is that the  $f_b$  parameters  $q_1, \dots, q_8$  do not depend on the top mass:

$$q_k = \beta_k. \tag{18}$$

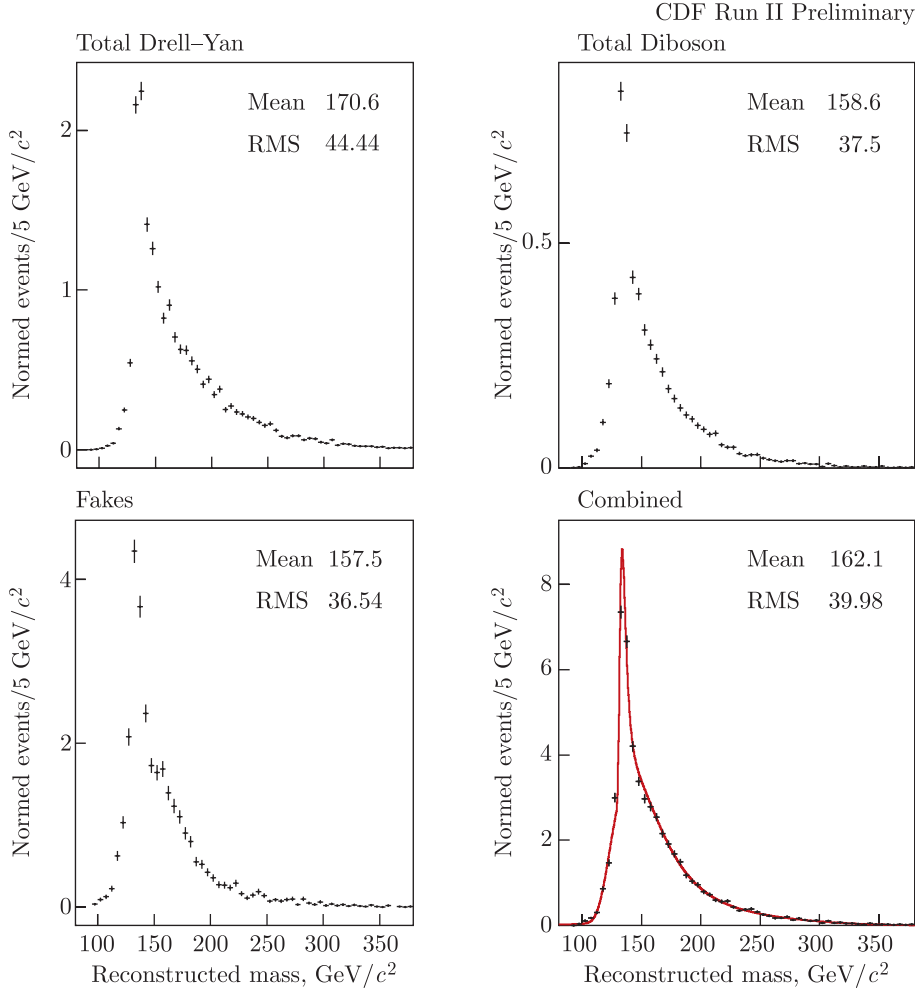


Fig. 8. Templates of background processes Drell-Yan, Diboson, «fake» events. Lower right plot shows the combined background

## 6. RESULTS FROM PSEUDO-EXPERIMENTS

We checked whether the fit with likelihood form (11) was able to return the correct mass by performing the «sanity check» pseudo-experiments for different input top mass values.

The numbers of signal and background events in PEs were Poisson distributed with mean values as their expected numbers. We took, as expected, numbers  $108.95 \pm 3.38$  and  $97.18 \pm 11.88$  for signal and background, respectively. These values were obtained using scaling from 1.1 to  $2 \text{ fb}^{-1}$ .

The output  $M_{\text{top}}$  (median of distribution) vs. input  $M_{\text{top}}$  is shown in Fig. 9, left.

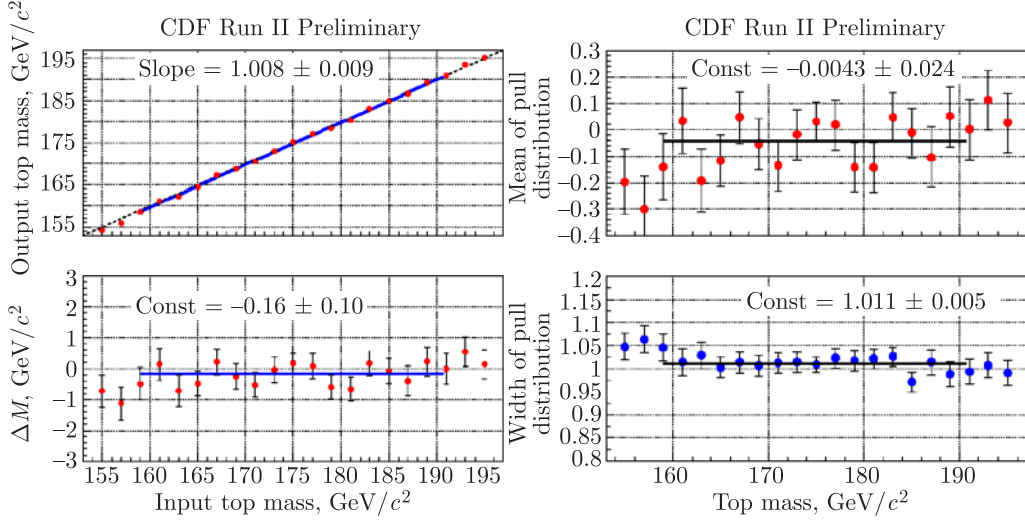


Fig. 9. Left: The extracted top mass as a function of input mass. The result of a linear fit is also shown. The lower plot shows the residuals (differences between reconstructed and input top mass). Right: Mean (above) and  $\sigma$  (below) of pull distributions determined from the pseudo-experiments as a function of input top mass

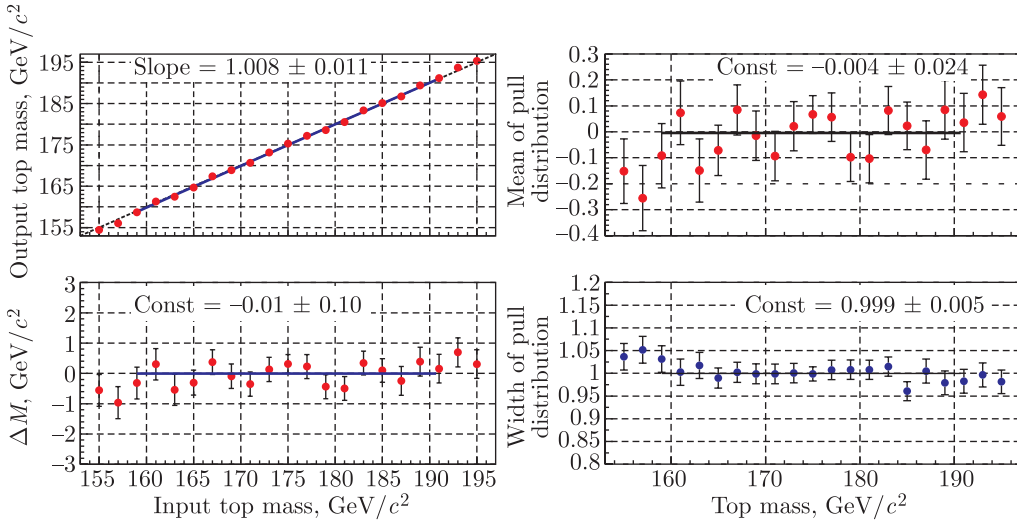


Fig. 10. Left: The extracted top mass as a function of input mass after applying the corrections for mean value and for errors. The result of a linear fit is also shown. The lower plot shows the residuals (differences between reconstructed and input top mass). Right: Mean (above) and  $\sigma$  (below) of pull distributions determined from the pseudo-experiments as a function of input top mass. Corrections for mean value and for errors are applied

A linear fit yielded a slope of  $1.008 \pm 0.009$ . The mean and width of the pull distributions as a function of input top mass are shown in Fig. 9, right.

The correction for the top mass mean value is  $0.16 \pm 0.10 \text{ GeV}/c^2$ . It is obtained from the fit of the distribution: residual vs. top mass (see Fig. 9, left).

The obtained correction for pull width is 1.011.

We checked the obtained corrections for top mass value and errors on the set of pseudo-experiments. The results are presented in Fig. 10.

One can see now that the residual is equal to 0.0 (Fig. 10, left) and the width of pull distribution is 1.0 (Fig. 10, right) in the framework of errors.

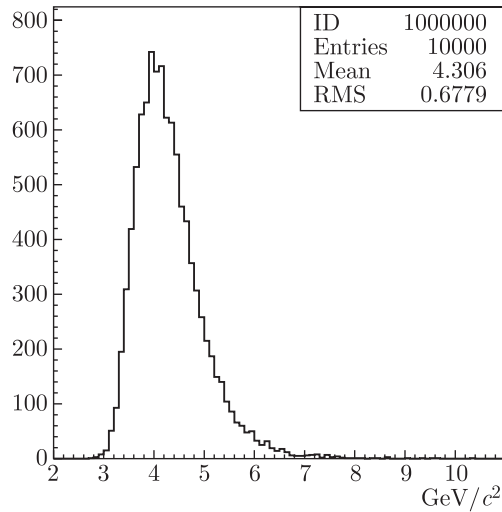


Fig. 11. Statistical error distribution for top mass measurement and MC sample with top mass  $175 \text{ GeV}/c^2$

We estimated the expected statistical error of top-quark mass measurement using MC sample with top mass  $175 \text{ GeV}/c^2$  (see Fig. 11). The error is expected to be  $4.3 \text{ GeV}/c^2$ , and taking into account the pull width correction we finally obtain  $4.4 \text{ GeV}/c^2$ .

## 7. BLIND TEST RESULTS

Before «opening the box» with data we performed test on the blind MC samples. The difference between extracted and true mass values for different blind samples in random order are shown in Table 2. The results are good: we have determined the top masses for blind samples with expected accuracy.

We present figures concerning the blind samples here. These are the distributions of residuals, statistical errors and pull of pseudo-experiments for determination of the blind top masses (see Fig. 12 ). The biases for the mean value (Fig. 13, left) and the pull width (Fig. 13, right) are also presented. We can stress that the bias in pull width conforms to the estimated one:  $1.011 \pm 0.005$ .

**Table 2. Results on the blind samples**

$M_{\text{rec}} - M_{\text{true}}, \text{GeV}/c^2$	Errors, $\text{GeV}/c^2$	Number of sigmas
0.6	1.2	0.5
-0.4	1.2	0.3
1.4	1.2	1.2
-0.9	1.2	0.8
0.3	1.2	0.2
1.4	1.2	1.1
0.3	1.2	0.3
0.0	1.2	0.0
-0.6	1.2	0.5
0.6	1.2	0.5

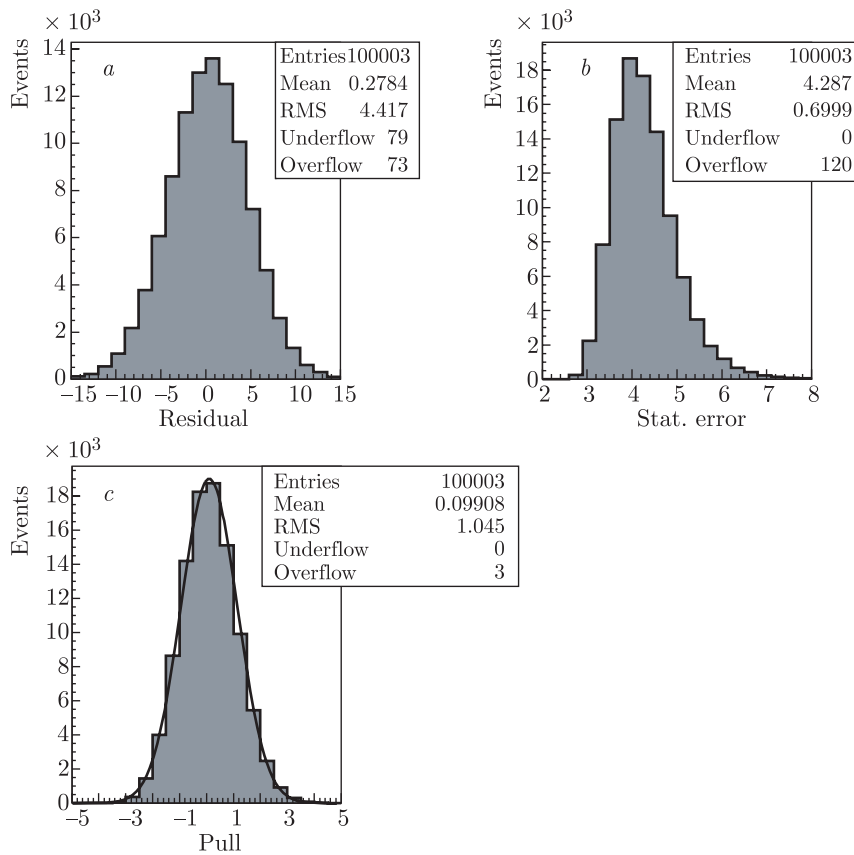


Fig. 12. Residuals (a), statistical errors (b) and pull distribution (c) for pseudo-experiments for determination of the blind top masses

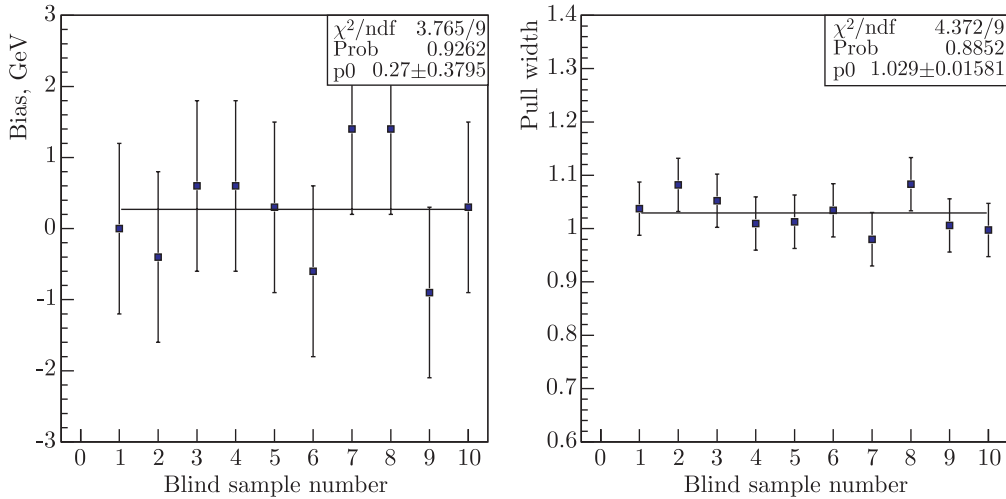


Fig. 13. Left: The bias for the blind samples top masses. Right: The bias in the pull width for the blind samples

## 8. SYSTEMATIC UNCERTAINTIES

We have considered the following sources of systematic uncertainties on the fitted mass value: a) jet energy scale, b) amount of initial and final state radiation, c) shape of the background template, d) parton distribution functions, e) approximations made by Monte Carlo generators, f)  $b$ -jet energy scale and lepton energy scale. The magnitudes of these uncertainties were estimated using large Monte Carlo samples generated only for the systematic study.

The procedure for estimating the systematic uncertainty is similar for all sources. For each source we varied the input value as appropriate (by  $1\sigma$ , or changing PDF, etc.) and evaluated the impact on the returned top mass. This was done by simulating a large number (usually 10000 or more) of pseudo-experiments (PE) with the nominal assumption and with the alternate assumption. The reconstructed mass distribution from each PE was fitted with the same likelihood procedure. The obtained mass value was entered into an ensemble of results of simulated experiments. The systematic uncertainty assigned to our measurement is the difference in the average of these result distributions for the nominal and shifted ensembles or half the difference between results obtained with  $+\sigma$  and  $-\sigma$  of the corresponding parameter change.

**8.1. Jet Energy Scale.** In Run 2 the jet systematic uncertainty is included in the jet correction software package. It is possible to turn on a  $\pm 1\sigma$  change in the energy scale for the specific type of jet correction.

By means of the above-described PE we estimated the mass shift caused by different corrections. We obtained the overall uncertainty of  $2.9 \pm 0.03 \text{ GeV}/c^2$  shifting jets in both signal and background MC events by  $\pm\sigma$  of the total jet energy systematic uncertainty.

Individual contributions to the systematic uncertainty are presented in Table 3.

**Table 3. Mass shifts indicated by the PE when the jet energy is shifted by  $\pm 1\sigma$  of each separate correction**

Level	Source	$M_{\text{rec}} \text{ GeV}/c^2$		Uncertainty $\text{GeV}/c^2$
		$+\sigma$	$-\sigma$	$\Delta M_{\text{rec}}/2$
1	$\eta$ -dependent	175.80	174.58	$0.61 \pm 0.03$
4	Multiple interactions	175.20	175.16	$0.02 \pm 0.03$
5	Absolute scale	177.26	172.93	$2.17 \pm 0.03$
6	Underlying event	175.37	175.05	$0.16 \pm 0.03$
7	Out-of-cone	176.99	173.36	$1.81 \pm 0.03$
8	Splash-out	175.49	174.94	$0.28 \pm 0.03$
Total	Sum in quadrature			$2.91 \pm 0.07$
100	Altogether sources	177.95	172.17	$2.88 \pm 0.03$
<b>Total</b>				<b>2.9</b>

**8.2. Radiation Effects, Generators and  $b$ -jet Energy Scale.** The effects of initial (ISR) and final (FSR) state radiation on the returned top mass were studied using Pythia as a signal generator. To estimate the uncertainty induced by ISR we studied the difference between ISR enhanced and reduced samples, as recommended by the top group. The half difference between average reconstructed top masses from these samples is assigned as a systematic uncertainty from ISR. To estimate the uncertainty induced by FSR we used the Pythia with enhanced and with reduced amount of FSR.

The results for the ISR and FSR induced systematics are summarized in Table 4.

**Table 4. Top mass shifts obtained from the PE for different Monte Carlo samples**

Source		Datasets	Mass, $\text{GeV}/c^2$	Mass shift, $\text{GeV}/c^2$	Syst., $\text{GeV}/c^2$
$b$ -JES	$\pm 1\%$ shift in JES for $b$ -jets	tkt75(-) tkt75(+)	$174.15 \pm 0.04$ $176.24 \pm 0.04$	$\Delta M/2 = 1.04 \pm 0.03$	0.62
Gener.	Herwig Pythia	htop75 tkt75	$174.71 \pm 0.32$ $175.17 \pm 0.15$	$\Delta M = 0.46 \pm 0.35$	0.46
ISR	More ISR Less ISR	itoprk itopr1	$175.00 \pm 0.32$ $174.95 \pm 0.32$	$\Delta M = -0.17 \pm 0.34$ $\Delta M = -0.22 \pm 0.34$	0.34
FSR	More FSR Less FSR	ftoprj ftopr1	$175.05 \pm 0.32$ $175.38 \pm 0.32$	$\Delta M/2 = 0.17 \pm 0.22$	0.22

The effect of using different top Monte Carlo generators was checked by comparing nominal Pythia with Herwig samples. The obtained mass shifts are presented in Table 4.

**8.3. Background Shape. *Background composition.*** In order to estimate effect on top mass from the uncertainty in background composition we varied

the contribution in combined background template of main sources (Diboson, Drell–Yan and «fakes») by  $\pm\sigma$ . Contribution from the other subsamples was corrected to maintain the total expected number of background events. As a result, 6 alternative combined background templates were obtained and used for PEs. The obtained top mass shifts are presented in Table 5. We assigned

**Table 5. Top mass shifts obtained from the PE for different BG composition and fake shape**

Source		Mass, GeV/ $c^2$	Mass shift, GeV/ $c^2$	Syst., GeV/ $c^2$
BG compos- ition	Diboson ( $-\sigma$ )	$175.15 \pm 0.04$	$\Delta M/2 = -0.02 \pm 0.03$	0.03
	Diboson ( $+\sigma$ )	$175.11 \pm 0.04$		
	DY ( $-\sigma$ )	$174.90 \pm 0.04$	$\Delta M/2 = 0.25 \pm 0.03$	0.25
	DY ( $+\sigma$ )	$175.40 \pm 0.04$		
	Fakes ( $-\sigma$ )	$175.53 \pm 0.04$	$\Delta M/2 = -0.39 \pm 0.03$	0.39
	Fakes ( $+\sigma$ )	$174.74 \pm 0.04$		0.46
Fake shape	–linear $E_T$ -dependent shift in fake rate matrix	$174.80 \pm 0.04$	$\Delta M/2 = 0.41 \pm 0.03$	0.41
	+linear $E_T$ -dependent shift in fake matrix	$175.61 \pm 0.04$		
Drell–Yan shape	decreased weight in the $Z$ window	$174.88 \pm 0.04$	$\Delta M/2 = 0.30 \pm 0.03$	0.30
	increased weight in the $Z$ window	$175.48 \pm 0.04$		

0.46 GeV/ $c^2$  as our systematic error for composition in combined background template.

**«Fake» events template shape.** In order to study how the uncertainty for «fake» events template shape can affect our resulting top mass we inserted linear  $E_T$ -dependent shift for values in our fake rate matrix.

Two new fake templates were obtained using changed fake rate matrix and included in combined background template. Using these templates for PEs we got shifts in top mass as presented in Table 5. We took 0.41 GeV/ $c^2$  as our systematic error for uncertainty in template for «fake» events shape.

**Drell–Yan template shape.** In order to suppress Drell–Yan events ( $Z/\gamma^* \rightarrow ee, Z/\gamma^* \rightarrow \mu\mu$ ) we have the increased requirement on missing  $E_T$  for events with effective mass of lepton and track lepton inside  $Z$  window ( $Z$ -veto cut). Drell–Yan events can get significant value of missing  $E_T$  only because mismeasurement of  $E_T$  jets. Differences between modeling of this effect and the reality can give us the shifted top mass. In order to estimate the sensitivity of our measurement to this we increased (and decreased) by the factor of 2 the weight in  $Z/\gamma^* \rightarrow ee, Z/\gamma^* \rightarrow \mu\mu$  templates for events which have effective mass of lepton and track lepton inside  $Z$  window. Two new combined background templates were obtained using this changed  $Z/\gamma^* \rightarrow ee, Z/\gamma^* \rightarrow \mu\mu$  templates.

Then we got from PEs the shifts in the top mass as presented in Table 5. We took  $0.3 \text{ GeV}/c^2$  as our systematic error due to uncertainty in Drell–Yan template shape.

**8.4. Parton Distribution Functions.** The uncertainty induced by PDFs was assessed by comparing CTEQ5L vs. MRST with Pythia. The results are listed in Table 6. The recently developed next-to-leading order PDF from CTEQ6

**Table 6. PDF Systematics**

Source	Mass shift, $\text{GeV}/c^2$	Syst., $\text{GeV}/c^2$
CTEQ PDFs	Sum $(\Delta M/2) = 0.21 \pm 0.13$	0.21
CTEQ5L vs. MRST72	$\Delta M = 0.07 \pm 0.06$	0.07
$\alpha_s$ (MRST72 vs. MRST75)	$\Delta M = -0.22 \pm 0.06$	0.22
Total		0.31

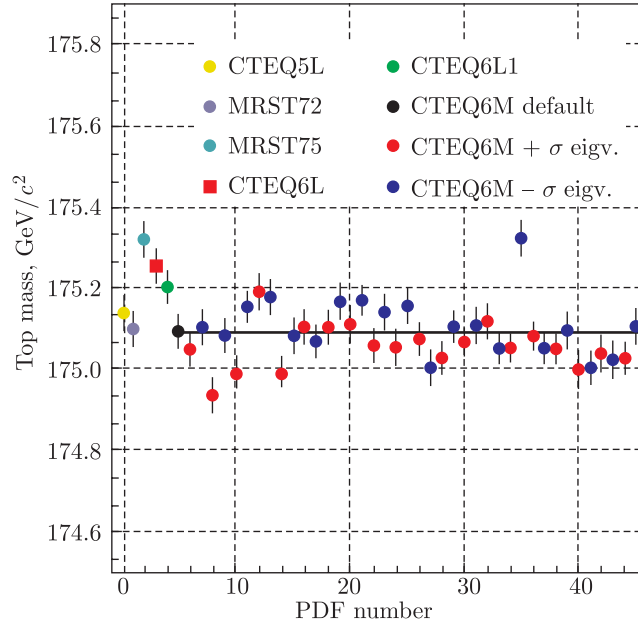


Fig. 14. Results used for PDF uncertainty

allows us to vary some PDF sets within their uncertainty. The possible variations are separated into contributions from 20 independent eigenvectors, so in total we have 41 different sets (1 nominal and  $2 \times 20$  for  $\pm 1\sigma$  variations). The PDF effect is studied using the reweighting method, where reconstructed top mass templates for each PDF set are obtained from one single sample (Pythia  $175 \text{ GeV}/c^2$  sample) by weighting the mass for each event by the probability for that event to proceed according to the given PDF. Results for the nominal PDF and for the

20 pairs of  $\pm 1\sigma$  PDFs are shown in Fig. 14. The black line corresponds to the nominal PDF set. The total PDF uncertainty was estimated as  $0.31 \text{ GeV}/c^2$ .

**8.5. Lepton Energy Scale.** The effect on the top mass from the uncertainty on lepton energy scale was studied by applying  $\pm 1\%$  shifts for lepton  $p_T$ . Resulting top masses are  $175.48 \text{ GeV}/c^2$  and  $174.84 \text{ GeV}/c^2$ . We take the half difference ( $0.3 \text{ GeV}/c^2$ ) as our systematic error from lepton energy scale uncertainty (see Table 7).

**8.6. Summary of Systematic Errors.** The summary of systematic uncertainties are listed in Table 7. For each source of systematic uncertainty we choose the obtained from PE mass shift or its error, whichever one is bigger.

**Table 7. Summary of systematic uncertainties**

CDF Run II Preliminary

Source	Uncertainty, $\text{GeV}/c^2$
Jet energy scale	2.9
<i>b</i> -JES	0.6
Initial state radiation	0.3
Final state radiation	0.2
Parton distribution functions	0.3
Monte-Carlo generators	0.5
Background composition	0.5
Fakes shape	0.4
DY shape	0.3
Lepton energy scale	0.3
<b>Total</b>	<b>3.1</b>

## 9. DATA

The data sample we used in our analysis includes data collected between March 2002 and May 2007 and corresponds to a total integrated luminosity of  $2.1 \text{ fb}^{-1}$ .

We selected 236 top event candidates. The background was rescaled from track + lepton cross-section measurement at  $1.1 \text{ fb}^{-1}$ , and the estimated value is  $N_b = 105.8 \pm 12.9$ .

The two-component background-constrained fit ( $N_b = 105.8 \pm 12.9$ ) for the obtained l + trk sample returns:  $M_{\text{top}} = 167.57 \pm_{3.99}^{4.15} \text{ GeV}/c^2$ , with  $126.13 \pm_{17.41}^{17.99}$  signal events and  $108.3 \pm_{11.5}^{11.6}$  background events.

The fitted mass distribution is shown in Fig. 15. The insert shows the mass dependence of the negative log-likelihood function.

We also performed a fit when the number of the background events was unconstrained (see Fig. 16). This fit returns  $M_{\text{top}} = 167.59 \pm_{4.21}^{4.42} \text{ GeV}/c^2$ , with  $117.82 \pm_{26.59}^{26.48}$  signal events and  $118.18 \pm_{25.52}^{27.53}$  background events.

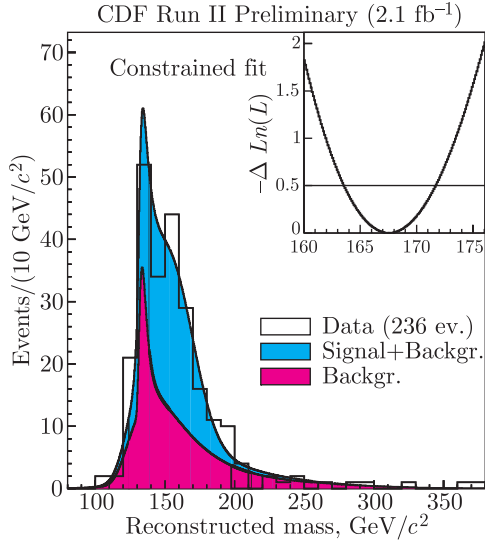


Fig. 15. Two-component constrained fit to the  $l+\text{trk}$  sample. The pink solid area corresponds to the background returned by the fit and the blue area is the sum of background and signal events. The insert shows the mass-dependent negative log-likelihood used in the fit

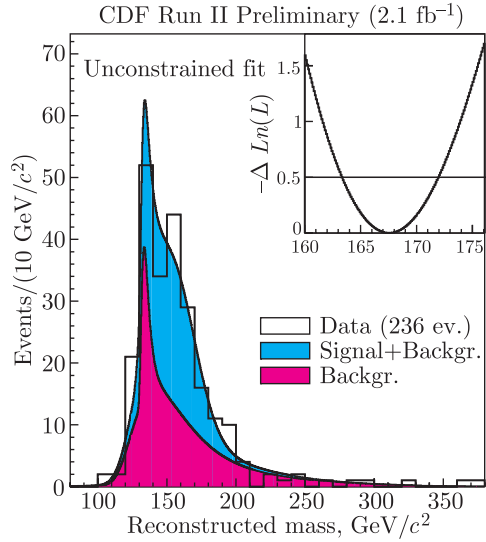


Fig. 16. Two-component unconstrained fit to the  $l+\text{trk}$  sample. The pink solid area corresponds to the background returned by the fit and the blue area is the sum of background and signal events. The insert shows the mass-dependent negative log-likelihood used in the fit

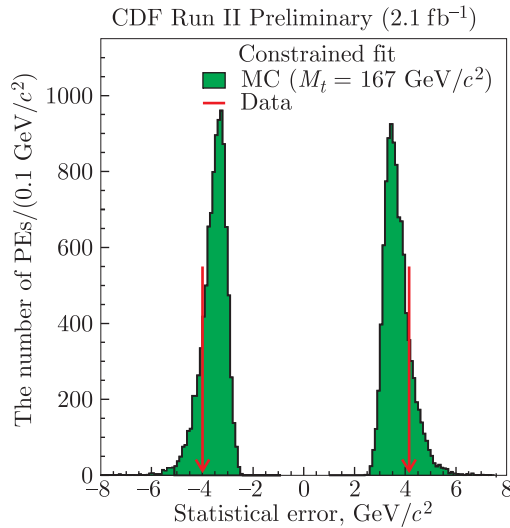


Fig. 17. Expected statistical errors for different top masses. The arrows indicate the errors returned by the fit to the data

Expected statistical errors obtained from the pseudo-experiments are shown in Fig. 17. The plot shows the statistical error distribution for the top mass of

167 GeV/ $c^2$ . The arrows indicate the errors returned by the fit to the data. The probability to have better accuracy than one from our data is 83%.

## 10. CONCLUSION

We applied the neutrino  $\phi$  weighting method to solve a non-constrained kinematics of the top quark decay in dilepton mode.

The 236 candidate events were selected from the data sample with integrated luminosity of 2.1 fb $^{-1}$ . Our preliminary measurement of the top quark mass in the l+trk sample is:  $M_{\text{top}} = 167.7 \pm_{4.0}^{4.2}$  (stat.)  $\pm 3.1$  (syst.) GeV/ $c^2$ . Statistical errors are shown here after multiplying by the factor of 1.011 and the mean value increased on 0.16 GeV/ $c^2$  — the values obtained from our pseudo-experiments.

## APPENDIX

We show the kinematical distributions which have been obtained to validate our data sample for CDF integrated luminosity of 2.1 fb $^{-1}$ . The distributions for  $N_{\text{jet}} \geq 2$  events were obtained on the data sample selected for our top mass measurement. The distributions for  $N_{\text{jet}} = 0$  and  $N_{\text{jet}} = 1$  events were obtained on the data sample with relaxed cuts on the number of jets per event.

Figure 18 shows the comparison between observed and predicted numbers of events. The number of predicted events (see Figs. 19–24) is scaled to be equal to the number of observed ones. The relative backgrounds and signal contribution for predicted events are taken according to the  $x$ -section group measurements.

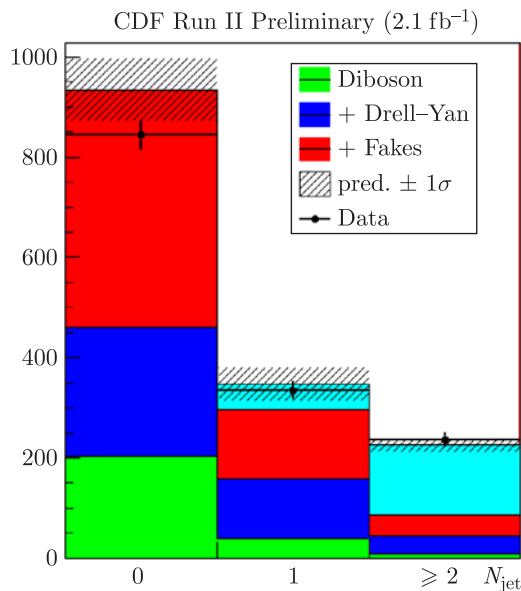


Fig. 18. Number of predicted events compared to the number observed in the data. The shaded areas show the ( $1\sigma$ ) uncertainties on the predicted numbers

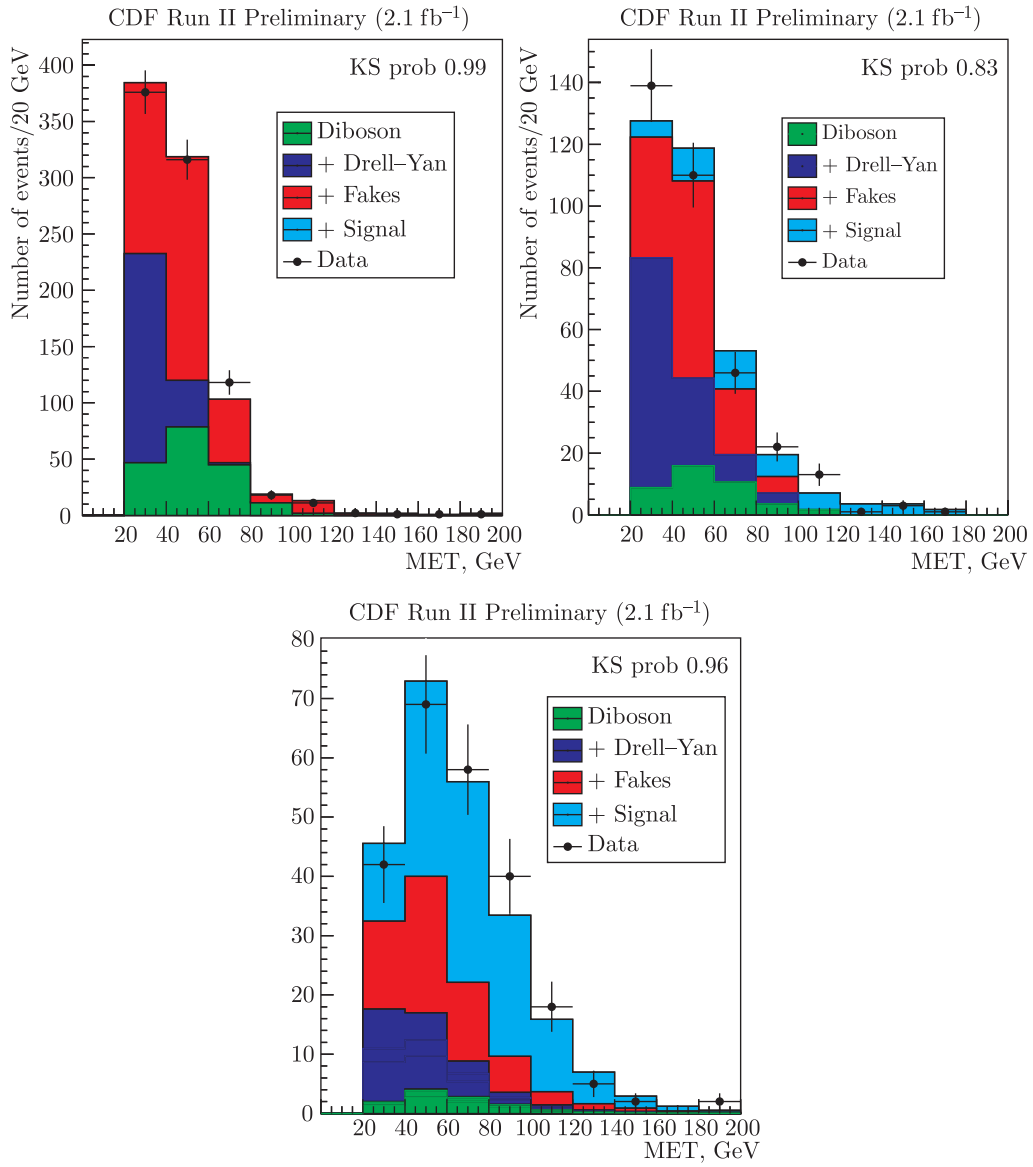


Fig. 19. Missing  $E_t$  distribution of predicted and candidate events. The plots are for different number of jets in the events. Top left:  $N_{\text{jet}} = 0$ , top right:  $N_{\text{jet}} = 1$ , bottom:  $N_{\text{jet}} \geq 2$

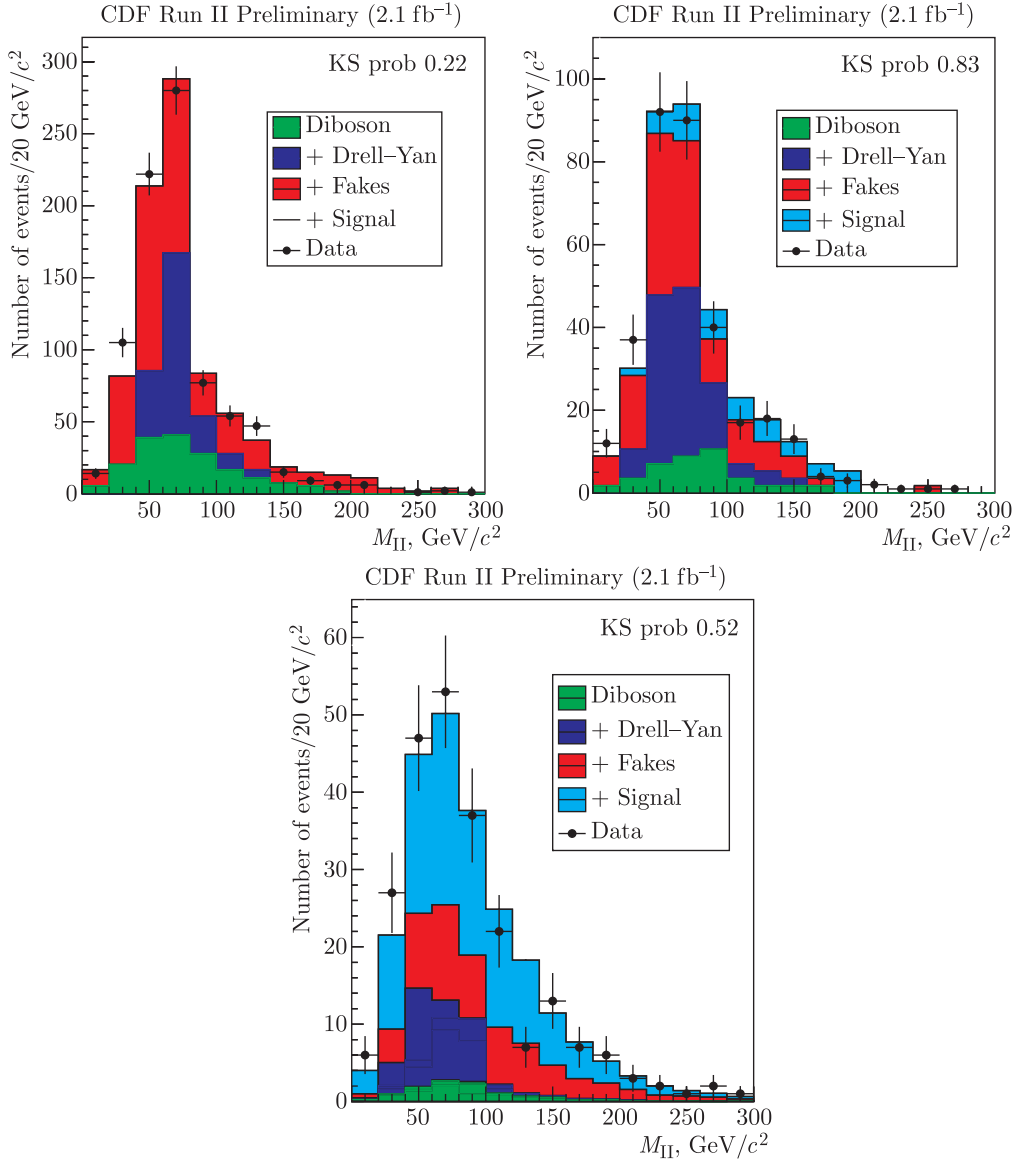


Fig. 20. Invariant mass of the tight lepton-track lepton pair in predicted and candidate events. The plots are for different number of jets in the events. Top left:  $N_{\text{jet}} = 0$ , top right:  $N_{\text{jet}} = 1$ , bottom:  $N_{\text{jet}} \geq 2$

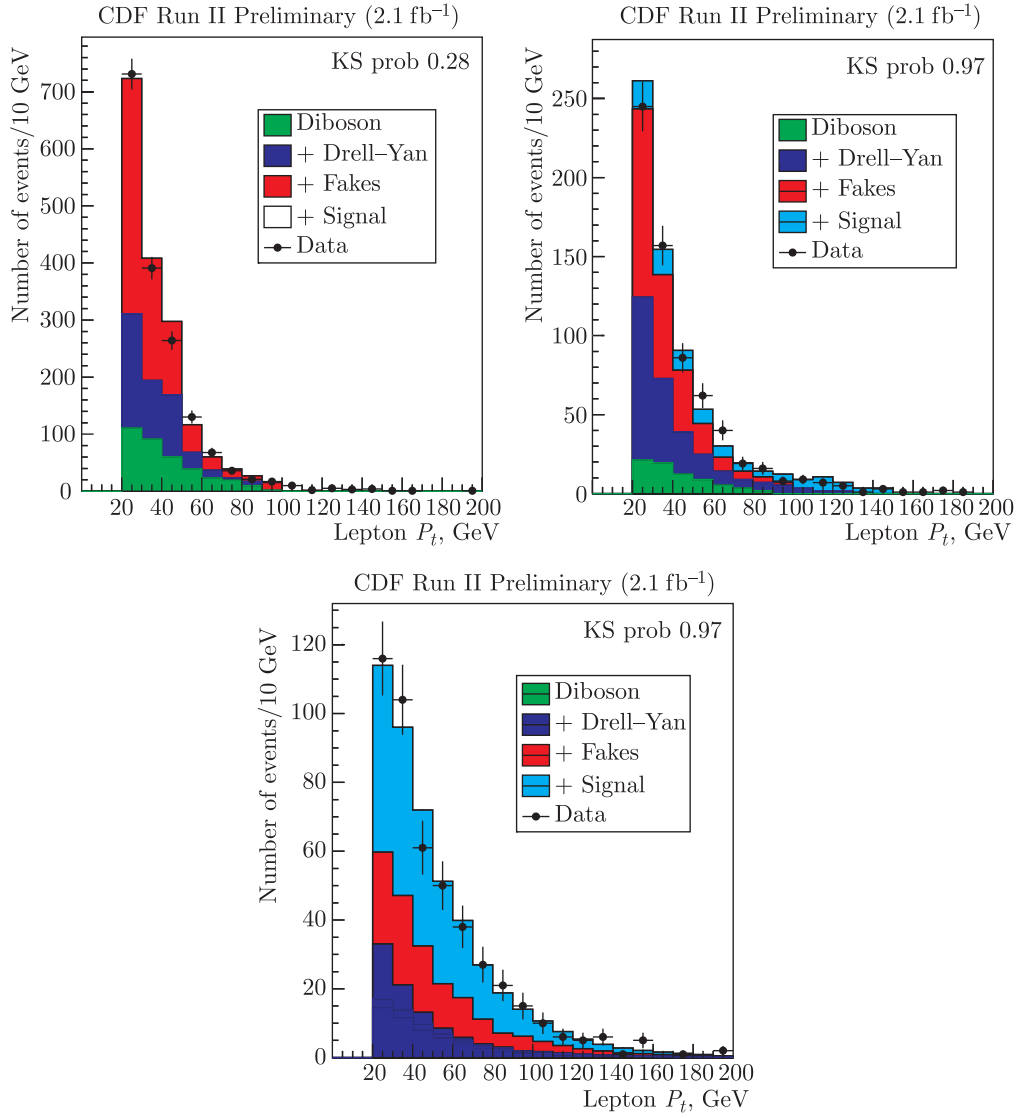


Fig. 21. Transverse momentum of both lepton candidates in predicted and candidate events. The plots are for different number of jets in the events. Top left:  $N_{\text{jet}} = 0$ , top right:  $N_{\text{jet}} = 1$ , bottom:  $N_{\text{jet}} \geq 2$

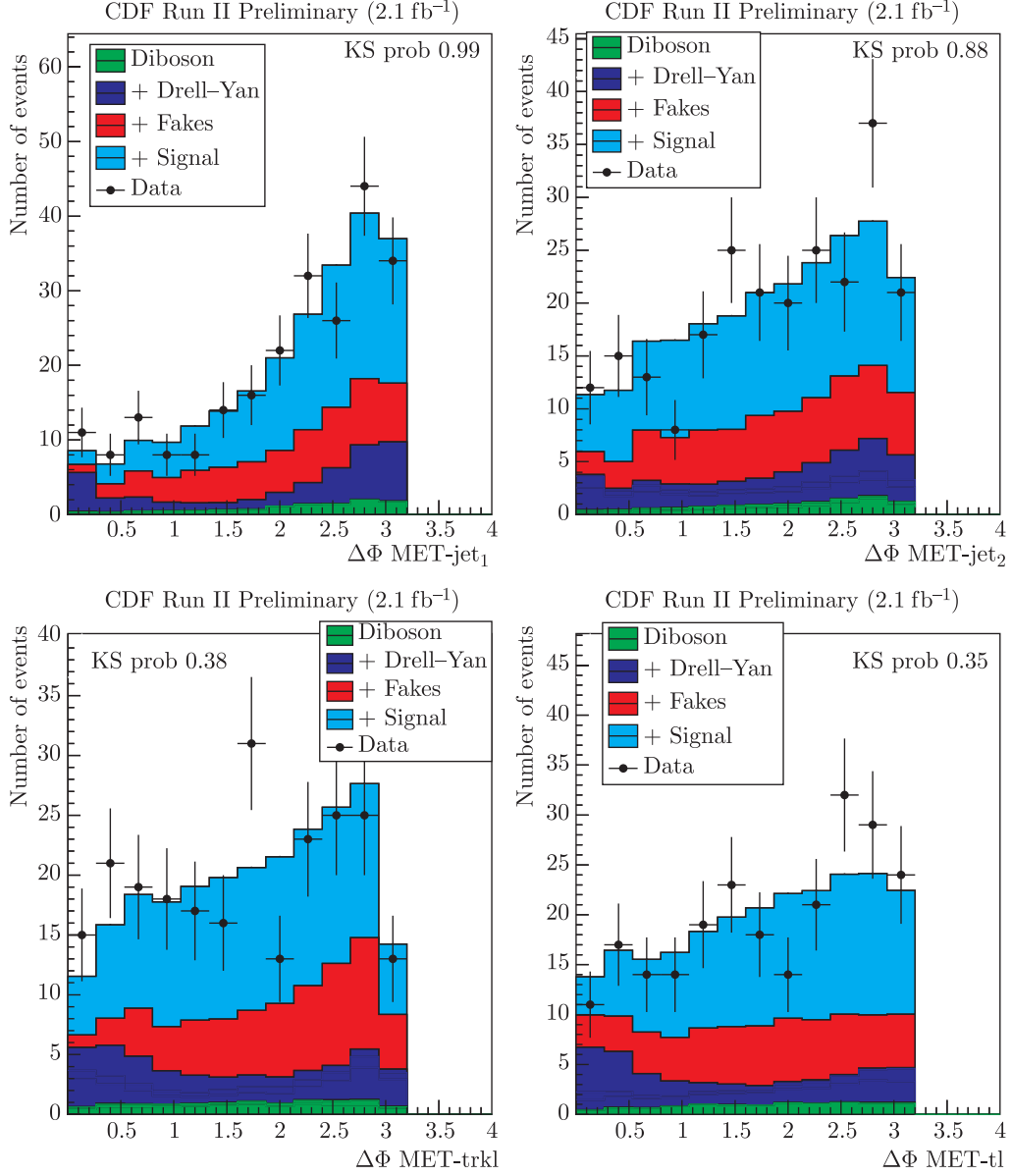


Fig. 22. These distributions are for number of jets in the events  $N_{\text{jet}} \geq 2$ . Upper left plot:  $\Delta\phi$  between missing  $E_t$  and leading  $E_t$  jet. Upper right plot:  $\Delta\phi$  between missing  $E_t$  and second leading  $E_t$  jet. Bottom left plot:  $\Delta\phi$  between missing  $E_t$  and isolated track. Bottom right plot:  $\Delta\phi$  between missing  $E_t$  and tight lepton

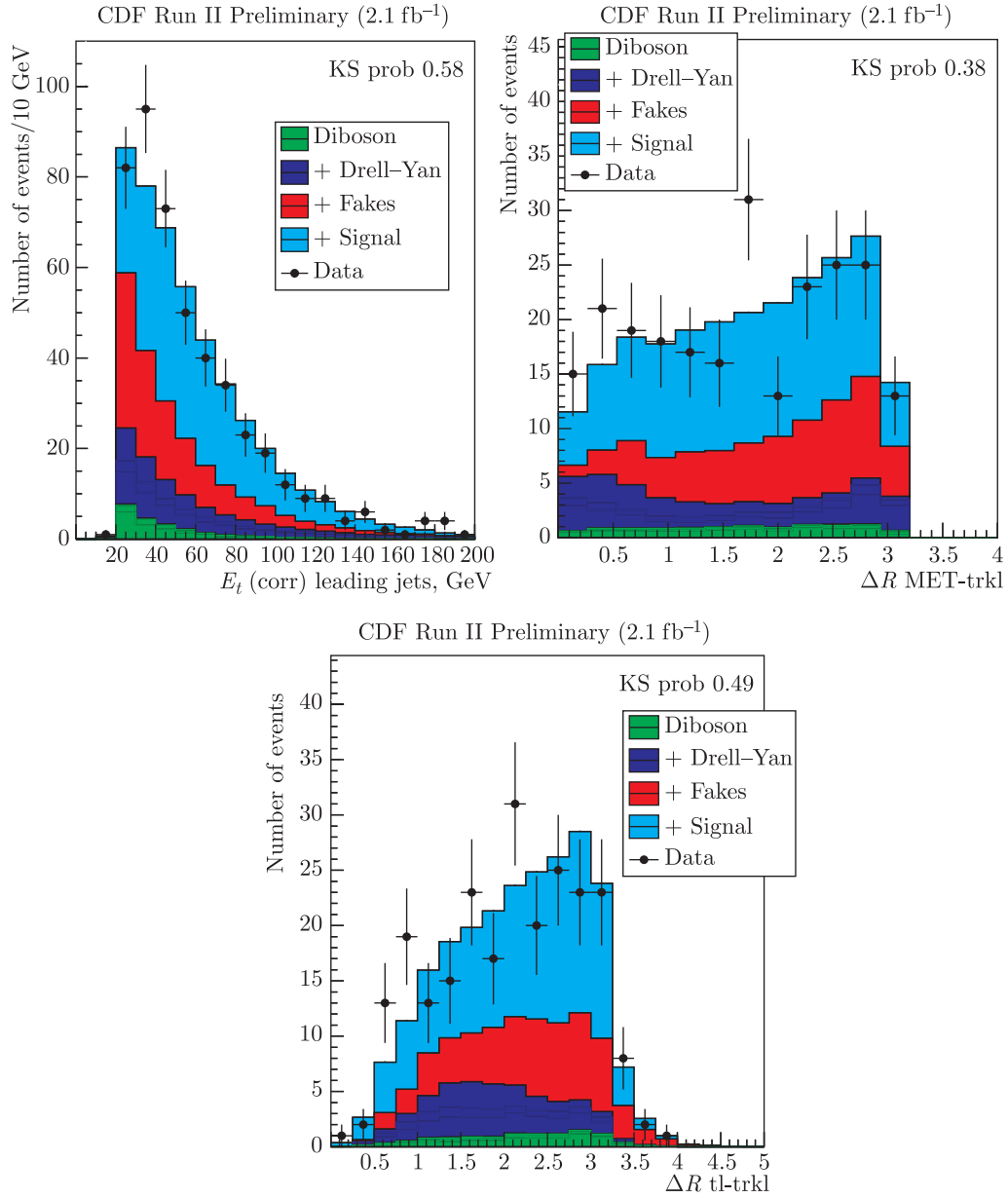


Fig. 23. These distributions are for number of jets in the events  $N_{\text{jet}} \geq 2$ . Upper left plot:  $E_t$  distribution of the leading jet. Upper right plot:  $\Delta R$  between missing  $E_t$  and isolated track. Bottom plot:  $\Delta R$  between tight lepton and isolated track

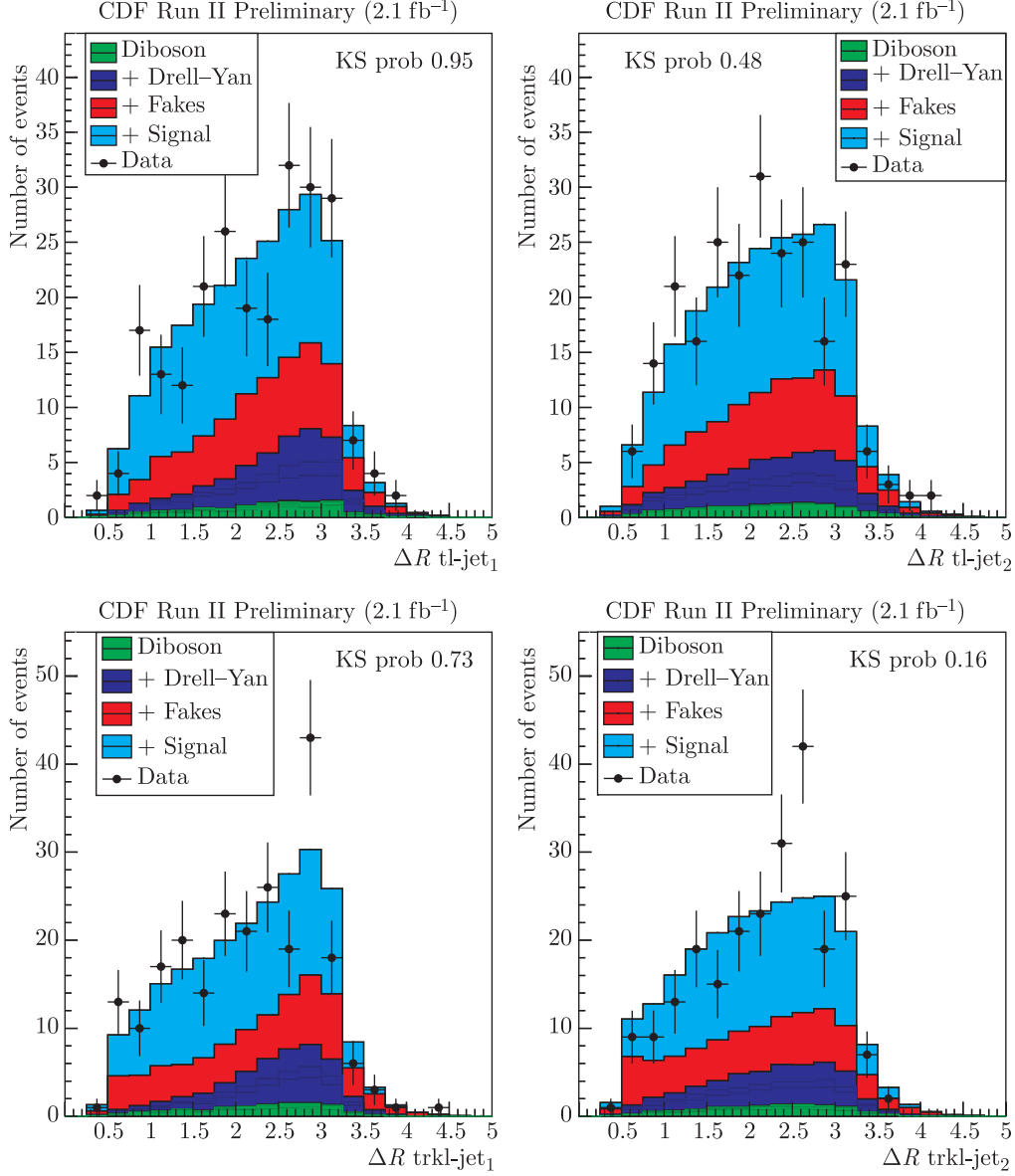


Fig. 24. These distributions are for number of jets in the events  $N_{\text{jet}} \geq 2$ . Upper left plot:  $\Delta R$  between tight lepton and leading  $E_t$  jet. Upper right plot:  $\Delta R$  between tight lepton and second leading  $E_t$  jet. Bottom left plot:  $\Delta R$  between isolated track and leading  $E_t$  jet. Bottom right plot:  $\Delta R$  between isolated track and second leading  $E_t$  jet

## References

1. *CDF Collaboration*. Measurement of the Top Quark Mass Using Template Methods on Dilepton Events in Proton–Antiproton Collisions at  $\sqrt{s} = 1.96$  TeV // *Phys. Rev. D*. 2006. V. 73. P. 112006.
2. *Acosta D. et al.* // *Phys. Rev. D*. 2005. V. 71. P. 032001. The CDF II Detector Technical Design Report. Fermilab Report No. Fermilab-Pub-96/390-E.
3. *Yao W.-M. et al.* 2006 Review of Particle Physics // *J. Phys. G*. 2006. V. 33. P. 1.

Received on January 25, 2008.

## CONTENTS

1. Introduction	1
2. Principles of the Method	1
2.1. Constrained Variables	1
2.2. Fitter Procedure	1
2.2.1. The $\chi^2$ form	1
2.2.2. Scanning of the $(\phi_1, \phi_2)$ plane	3
2.2.3. Weighting the solutions	4
2.3. Picking up the Solution	5
2.4. Likelihood Form	5
3. PHI Method Optimization	6
4. Event Selection	8
5. Templates	10
5.1. Monte Carlo Signal Templates	10
5.2. Background Template	11
6. Results from Pseudo-Experiments	13
7. Blind Test Results	15
8. Systematic Uncertainties	17
8.1. Jet Energy Scale	17
8.2. Radiation Effects, Generators and $b$ -jet Energy Scale	18
8.3. Background Shape	18
8.4. Parton Distribution Functions	20
8.5. Lepton Energy Scale	21
8.6. Summary of Systematic Errors	21
9. Data	21
10. Conclusion	23
Appendix	23
References	30

Корректор *Т. Е. Попеко*

Подписано в печать 27.03.2008.

Формат 70 × 100/16. Бумага офсетная. Печать офсетная.

Усл. печ. л. 2,18. Уч.-изд. л. 3,22. Тираж 390 экз. Заказ № 56123.

Издательский отдел Объединенного института ядерных исследований  
141980, г. Дубна, Московская обл., ул. Жолио-Кюри, 6.

E-mail: [publish@jinr.ru](mailto:publish@jinr.ru)

[www.jinr.ru/publish/](http://www.jinr.ru/publish/)